Structural Eng./Earthquake Eng. Vol. 8, No. 1, 11s—20s, April 1991
Japan Society of Civil Engineers (Proc. of JSCE No. 428/ I —15)

ELASTIC BUCKLING STRENGTH AND POST-BUCKLING BEHAVIOR OF A PANEL UNDER UNEQUAL BENDING AND SHEAR

Masatoshi NAKAZAWA*, Tetsuo IWAKUMA**
and Shigeru KURANISHI***

The main objective is to investigate analytically the elastic interactive buckling strength and the post-buckling behavior of a simply supported panel subjected to combined loading of bending and shear. Special attention is paid to the effect of unequal end moments at both-side of a panel, which appear in the actual girder structures. The buckling modes are found to be governed mostly by the shear buckling mode. A simple-form formula to predict the buckling coefficients under combined unequal end moments and shear is proposed for the practical use. Moreover, the elastic post-buckling behavior and stress distribution are also discussed.

Keywords: *combined loading, interactive buckling strength, post-buckling behavior, Galerkin's method*

1. INTRODUCTION

A large amount of experimental and theoretical works have been carried out to investigate the behavior of panels in a plate girder subjected to shear forces and bending moments, and many useful findings have been accumulated. Although it is possible in the actual girder structures that a girder section is subjected to bending moment alone, the pure shear loading state never exists, because the shear force in a beam theory is equilibrated with the rate of change of the bending moment distribution. In other words, the existence of shear forces essentially requires non-uniform bending moment distribution in the longitudinal direction. Thus, most of the panels in the real plate girder structures are usually subjected to combined loading of bending moments and shear forces. Therefore, the true strength of plate girder must be discussed under these combined loading conditions.

Stein[1], Chwalla[2], Timoshenko[3] and Way[4] have presented the interactive buckling strength diagrams of a simply supported panel, but they are limited to apply for the cases of the equal end moments and shear forces. This unrealistic but simple loading condition is employed probably for a conservative estimate. Another researchers[5)~9)] carried out the buckling analysis of web panels under different loading conditions and boundary conditions.

On the other hand, Radulović[10] investigated the elastic buckling stress of a rectangular flat plate under the combined action of unequal end moments and normal force, which vary linearly in both directions. Galerkin's method is applied to the fundamental equation by Kármán under Navier's boundary condition for simply supported edges. He extended this analysis to a rectangular plate reinforced by a system of transverse elastic stiffeners[11]. Moreover, this linear buckling problem is developed for a longitudinally stiffened rectangular plate[12] and both longitudinally and transversely stiffened plate[13] with the effect of torsional rigidity of stiffeners. Radulović presented the method of calculation in these papers, however the characteristics of the interactive buckling strength has not been discussed sufficiently.

Kutzelnigg[14] calculated the diagram of buckling coefficients for the unstiffened web plates of continuous I-girder under the action of unequal end moments and shear. However, the special attention is paid for the effect of torsional rigidity of flanges for the interactive buckling strength. The typical analytical models corresponds to the conventional loading case of pure bending and pure shear and to the case of end shear panel, and there are not intermediate cases.

Takeda *et al.*[15] studied the elastic buckling of plate girders loaded with the unequal end moments by the finite difference method. The simultaneous buckling of the flange and web is analyzed by means of the theory of orthotropic plates, and the relationships between the flexural and torsional rigidities of the flange and lateral buckling strength are investigated in detail.

Hence the actual interactive buckling strength of

* Member of JSCE, Dr. Eng., Research Associate, Department of Civil Engineering, Tohoku University (Aoba Sendai 980 JAPAN).
** Member of JSCE, Ph.D., Associate Professor, Dept. of Civil Eng., Tohoku University.
*** Member of JSCE, Dr. Eng., Professor, Dept. of Civil Eng., Tohoku University.

plate girder webs with unequal end moments and shear forces has not been evaluated sufficiently yet. In addition, the investigation of the post-buckling behavior of a panel subjected to such a loading does not exist at all. The main purpose of this study is to investigate analytically both the elastic buckling strength and post-buckling behavior of a web panel. Special attention is paid to the effect of the realistic combined loading of bending and shear in the actual plate girders. This analysis includes the combined case of pure bending and pure shear in order to compare with the case of unequal bending and shear. Moreover, the elastic post-buckling behavior, the stress distributions, and the principal stress distributions are discussed.

2. BUCKLING ANALYSIS OF A PANEL SUBJECTED TO COMBINED UNEQUAL BENDING AND SHEAR

(1) Governing equations for buckling analysis and critical moment

For the buckling analysis of a flat plate, it may be straightforward to examine the incremental changes of the strain energy and external work at a critical state when the plate is subjected to the in-plane stresses. Let $w(x, y)$ denote the out-of-plane incremental deflections of the middle plane at buckling. Then, the incremental strain energy ΔU induced by the bending of plates and the incremental external work ΔT done by the pre-existing stress components in the middle plane can be expressed in the following form[16] :

$$\Delta U=\frac{1}{2}D\int\int\left\{\left(\frac{\partial^2 w}{\partial x^2}+\frac{\partial^2 w}{\partial y^2}\right)^2 -2(1-\nu)\left[\frac{\partial^2 w}{\partial x^2}\frac{\partial^2 w}{\partial y^2}-\left(\frac{\partial^2 w}{\partial x\partial y}\right)^2\right]\right\}dxdy \quad \cdots\cdots(1\text{-a})$$

$$\Delta T=\frac{1}{2}t\int\int\left[\sigma_x\left(\frac{\partial w}{\partial x}\right)^2+\sigma_y\left(\frac{\partial w}{\partial y}\right)^2 +2\tau_{xy}\frac{\partial w}{\partial x}\frac{\partial w}{\partial y}\right]dxdy \quad \cdots\cdots(1\text{-b})$$

where t and $D\equiv Et^3/12(1-\nu^2)$ are the plate thickness and the flexural rigidity of the plate, respectively. E is Young's modulus and ν is Poisson's ratio. $\sigma_x(x, y)$, $\sigma_y(x, y)$ and $\tau_{xy}(x, y)$ are the in-plane stress components and are treated as applied forces. These stress components are related to the Airy stress function $F(x, y)$ as

$$\sigma_x=\frac{\partial^2 F}{\partial y^2},\quad \sigma_y=\frac{\partial^2 F}{\partial x^2},\quad \tau_{xy}=-\frac{\partial^2 F}{\partial x\partial y} \cdots(2\text{-a,b,c})$$

Let four sides of a rectangular plate in **Fig.1** are

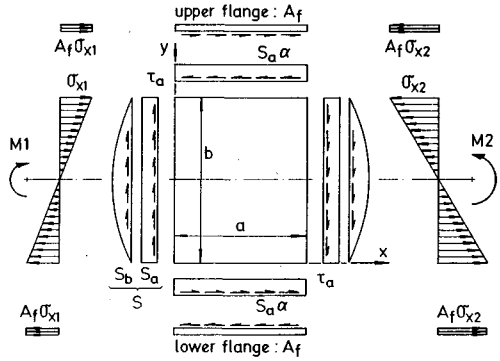

Fig.1 A web panel subjected to unequal end moments and shear force.

simply supported, and the buckled deflection can be assumed by a double-Fourier-series form as

$$w(x, y)=t\sum_{m=1}^{\infty}\sum_{n=1}^{\infty}b_{mn}\sin\left(\frac{m\pi x}{a}\right)\sin\left(\frac{n\pi y}{b}\right) \quad \cdots\cdots(3)$$

where m and n are the number of half-waves in the x- and y-direction, and b_{mn} are unknown coefficients to be determined.

The stress function $F(x, y)$ must be determined to satisfy the actual combined loading condition of the unequal end moments and shear along edges. We here consider a problem in which the plate is subjected to pure shearing stress and unequal bending moments M_1 and M_2 at both sides as shown in **Fig.1**. Then, the mechanical boundary conditions given by the stress resultant forces can be expressed as

$$M_1=-t\int_0^b\sigma_x(x=0)(y-\frac{b}{2})\,dy,$$

$$M_2=-t\int_0^b\sigma_x(x=a)(y-\frac{b}{2})\,dy \quad \cdots\cdots(4\text{-a,b})$$

$$\int_0^b\sigma_x dy=0 \quad \text{along } x=0,\ a \quad \cdots\cdots(4\text{-c})$$

$$\sigma_y=0 \quad \text{along } y=0,\ b \quad \cdots\cdots(4\text{-d})$$

$$\tau_{xy}=-\tau_a \quad \text{along } y=0,\ b \quad \cdots\cdots(4\text{-e})$$

where τ_a is the applied pure shearing stress component. The boundary conditions of Eqs. (4-a ~e) can be satisfied if the Airy stress function $F(x, y)$ is chosen as

$$F(x, y)=\tau_a\cdot xy-\frac{(2y^3-3by^2)}{b^3t}\left\{M_1+(M_2-M_1)\frac{x}{a}\right\}$$

$$=M_2\left[\frac{6\omega}{b^2t}xy-\frac{(2y^3-3by^2)}{b^3t}\left\{\gamma+(1-\gamma)\frac{x}{a}\right\}\right] \quad \cdots\cdots(5)$$

in which non-dimensional parameters

$$\gamma \equiv \frac{M_1}{M_2}, \quad \omega \equiv \frac{\tau_a}{\sigma_{x2}} = \frac{\tau_a b^2 t}{6M_2} \quad \cdots\cdots (6)$$

are introduced to express the applied loading ratios, where σ_{x2} is the maximum normal fiber stress at the right-hand-side edge. These parameters are not independent in the actual plate girder, and this relation is given by $\omega = (1-\gamma)\gamma_A/\alpha$, where γ_A is the ratio of cross-sectional area of flange plate A_f and web panel ; i.e. $\gamma_A = A_f/(bt)$. α is the aspect ratio defined by $\alpha \equiv a/b$. Although ω is the dependent parameter with γ as mentioned above, we adopt this one in order to cover the general cases including the conventional loading of pure bending and pure shear. Note that the substitution of Eq. (5) into Eq. (2-c) yields the parabolic distribution of the shear stress component along $x=0,a$ as shown in **Fig.1**.

Substitution of Eq. (3) into Eq. (1-a) yields

$$\Delta U = \frac{\pi^4 abt^2 D}{8} \sum_{m=1}^{\infty}\sum_{n=1}^{\infty} b_{mn}{}^2 \left(\frac{m^2}{a^2}+\frac{n^2}{b^2}\right)^2 \quad \cdots\cdots (7)$$

Similarly, by substituting Eqs. (2) and (3) into Eq. (1-b) using Eq. (5), we finally obtained

$$\begin{aligned}\Delta T = &-\frac{12t^2}{ab} M_2 (1+\gamma) \sum_{m=1}^{\infty}\left[\sum_{n=1}^{\infty}{}' \sum_{j}{}' b_{mn} b_{mj} \frac{m^2 nj}{(n^2-j^2)^2}\right] \\ &+ \frac{96t^2}{ab\pi^2} M_2 (1-\gamma) \sum_{m=1}^{\infty}\sum_{n=1}^{\infty} b_{mn} \cdot \\ &\left[\sum_{i}{}' \sum_{j}{}' b_{ij} \frac{mnij\,(m^2+i^2)}{(m^2-i^2)^2 (n^2-j^2)^2}\right] \\ &+ \frac{48t^2}{ab\pi^2} M_2 (1-\gamma) \sum_{m=1}^{\infty}\sum_{n=1}^{\infty} b_{mn} \cdot \\ &\left\{\sum_{i}{}' \sum_{j}{}' b_{ij} \left[\frac{mnij\,(n^2+3j^2)}{(i^2-m^2)(n^2-j^2)^3} \right.\right. \\ &\left.\left. + \frac{ijmn\,(j^2+3n^2)}{(m^2-i^2)(n^2-j^2)^3}\right]\right\} \\ &+ \frac{48t^2}{b^2} \omega M_2 \sum_{m=1}^{\infty}\sum_{n=1}^{\infty} b_{mn} \cdot \\ &\left[\sum_{i}{}' \sum_{j}{}' b_{ij} \frac{mnij}{(i^2-m^2)(n^2-j^2)}\right] \quad \cdots\cdots (8)\end{aligned}$$

where a prime on Σ indicates that the summation of i and j are taken only when $(m \pm i)$ or $(n \pm j)$ is odd.

The out-of-plane equilibrium condition requires that the incremental potential energy $(\Delta U - \Delta T)$ becomes stationary for given M_2. Therefore, all derivatives of $(\Delta U - \Delta T)$ with respect to all b_{mn}'s must vanish. As a result, the governing equations for the buckling analysis are obtained as

$$\begin{aligned}&b_{mn}(m^2+\alpha^2 n^2)^2 + \frac{48a^2}{b^2\pi^4}\lambda_{2cr}(1+\gamma)\sum_{j}{}' b_{mj}\frac{m^2 nj}{(n^2-j^2)^2} \\ &- \sum_{i}{}'\sum_{j}{}' b_{ij}\left\{\frac{192a^2}{b^2\pi^6}\lambda_{2cr}(1-\gamma)\left[\frac{2mnij\,(m^2+i^2)}{(m^2-i^2)^2(n^2-j^2)^2}\right.\right. \\ &\left. + \frac{mnij\,(n^2+3j^2)}{(i^2-m^2)(n^2-j^2)^3} + \frac{ijmn\,(j^2+3n^2)}{(m^2-i^2)(j^2-n^2)^3}\right] \\ &\left. + \frac{192a^3}{b^3\pi^4}\lambda_{2cr}\omega\frac{mnij}{(i^2-m^2)(n^2-j^2)}\right\} = 0 \\ &\text{for } m, n = 1, 2, 3, \cdots\cdots (9)\end{aligned}$$

where λ_{2cr} is the non-dimensional critical moment defined by

$$\lambda_{2cr} \equiv \frac{(M_2)_{cr}}{D} \quad \cdots\cdots (10)$$

Since Eq. (9) is a system of homogeneous equations for b_{mn}, the ordinary eigenvalue analysis for a non-trivial solution of b_{mn}'s determines the critical moment.

(2) Critical stresses

From the critical moment obtained in the preceding section, one can define the critical normal stress by the maximum value of σ_x as

$$\sigma_{2cr} \equiv \frac{6(M_2)_{cr}}{b^2 t} = \frac{6D}{b^2 t}\lambda_{2cr} \quad \cdots\cdots (11)$$

Let $\sigma_{cr}{}^*$ denote the critical stress in pure bending, and from Eqs. (6) and (11)

$$\sigma_{cr}{}^* \equiv \frac{6D}{b^2 t}\lambda_{2cr} \quad (\gamma=1, \omega=0) \quad \cdots\cdots (12)$$

In the next section, the buckling strength will be examined in terms of the non-dimensional critical stress using Eq. (12) ; i.e. $\sigma_{2cr}/\sigma_{cr}{}^*$.

It may be straightforward to define the critical shear stress by the critical value of τ_a from Eq. (6) ; i.e.

$$(\tau_a)_{cr} = \frac{6\omega}{b^2 t}(M_2)_{cr} = \frac{6\omega D}{b^2 t}\lambda_{2cr} = \omega\sigma_{2cr} \quad \cdots\cdots (13)$$

However, Eq. (13) does not take the effect of non-uniform bending moment into account. As is clear from substitution of Eq. (5) into Eq. (2-c), the shear stress distributes parabolically in the y-direction. This represents the shear component induced by the different end moments in a beam theory. Since the shear stress distribution in plate girder structures is calculated including this effect of non-uniform bending moment, it is reasonable to define the critical shear stress not by Eq. (13) but by the average shear stress acting along the y-axis as

$$(\tau_{av})_{cr} = \left(\frac{1}{b}\int_0^b \tau_{xy} dy\right)_{cr} = D\left\{\frac{1-\gamma}{abt} + \frac{6\omega}{b^2 t}\right\}\lambda_{2cr} \quad \cdots\cdots (14)$$

While the second term of Eq. (14) coincides with

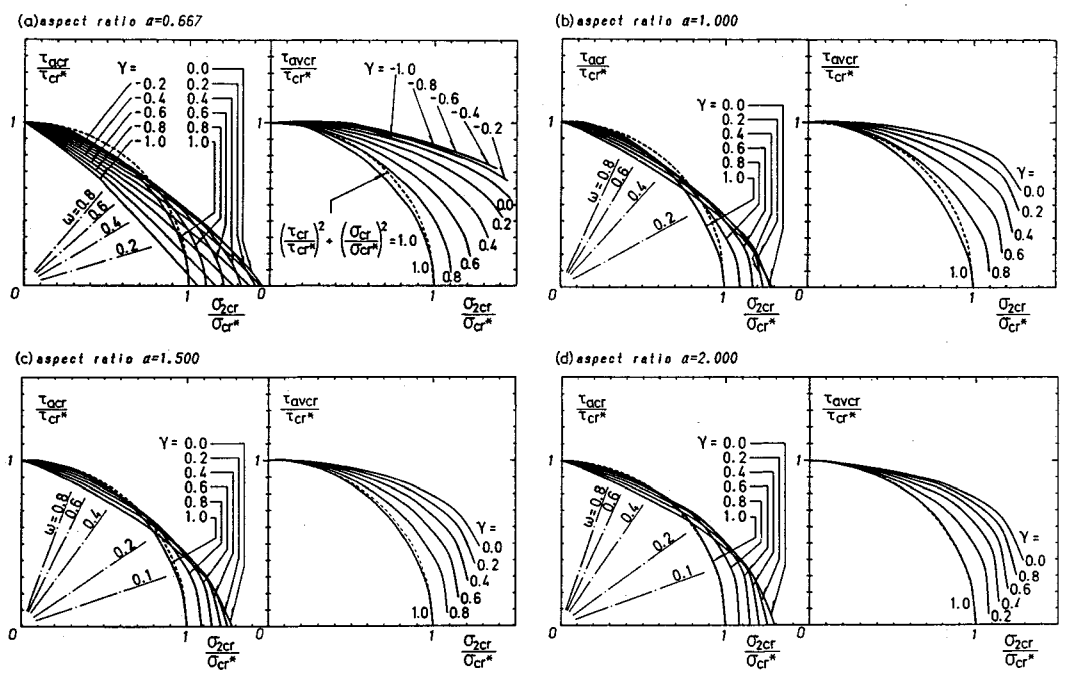

Fig.2 Interactive buckling strength diagram.

Eq. (13) and corresponds to the pure shearing part of the shear stress, the first term is the component which is in balance with non-uniform bending moment. Similarly to the normal critical stress, the shear stress is expressed in non-dimensional form by using the pure shear critical stress τ_{cr}^* defined by

$$\tau_{cr}^* = (\tau_a)_{cr} \quad \left(M_2=0,\ \omega\to\infty \text{ or } \omega\lambda_{2cr}\to\frac{b^2 t\,(\tau_a)_{cr}}{6D}\right) \qquad \cdots\cdots (15)$$

in the next section.

(3) Interactive buckling strength diagram

The buckling analysis of Eq. (9) is carried out for extensive combination of parameters. In the calculations, only the first 4 terms of each series are used basing on the examination of the convergency check. **Fig.2** (a) ~ (d) show typical interactive buckling strength diagrams. In these figures, coordinates are the non-dimensional critical stresses defined in the preceding section. As is clear from definitions in Eq. (6), γ is the ratio of end moments, and ω denotes the ratio of the applied shear stress and the bending fiber stress.

In **Fig.2** (a), when γ 0.0, interaction curves become almost straight in both diagrams in terms of τ_a and τ_{av}. This tendency holds for other values of aspect ratio α, because the shear force governs the buckling strength most in this range of γ. It can be also seen from the figures that the curve for $\gamma=$ 0.0 lies in the conservative side of all the critical states for $\gamma<0$, if the interaction curves are plotted in terms of τ_{av}. Therefore, in the following discussions, γ is limited within the range of $0.0\leqq\gamma\leqq1.0$. As a matter of fact, the actual range of parameters in the real plate girder structures may be $0.0\leqq\gamma\leqq1.0$ and $0.0\leqq\omega\leqq2\gamma_A$ when $\alpha\geqq0.5$.

In the figures using $(\tau_a)_{cr}$, for smaller ω, namely the bending moment is relatively dominant, the larger buckling strength is obtained. Moreover, the larger the difference of end moments becomes, the higher the interactive buckling strength becomes. Therefore, the conventional equation[17)~19)] shown by a dashed curve in the figures leads to a much more conservative design if the bending is larger than shear. On the contrary, for larger ω, namely when the shear force is relatively dominant, the interactive buckling strength becomes lower than the cases of the equal end moments owing to the secondary shear stresses induced by the increase of moment gradient. The larger difference of end moments yields the lower interactive buckling strength than the conventional equation. Therefore, we can not express the actual interactive buckling strength by the conventional equation using $(\tau_a)_{cr}$.

On the other hand, if the critical shear stress is adjusted by τ_{av} including the effect of unequal moments, the conventional circular curve almost lies in the conservative side of the critical buckling strength. The effect of unequal moments is taken

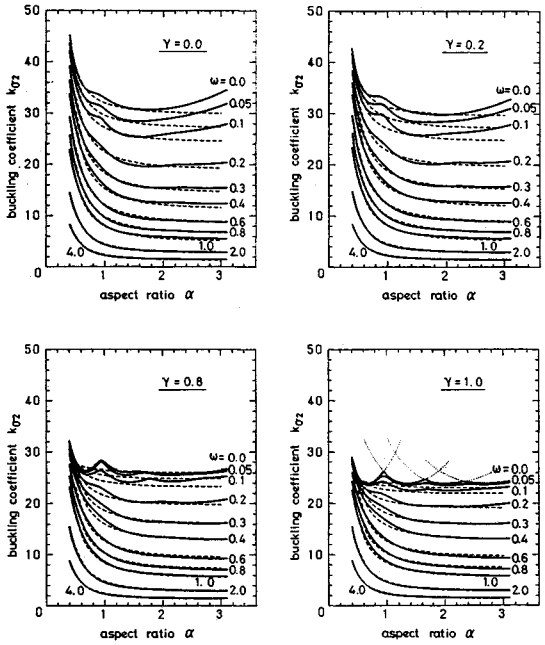

Fig.3 Relationships between buckling coefficients $k_{\sigma 2}$ and aspect ratio α.

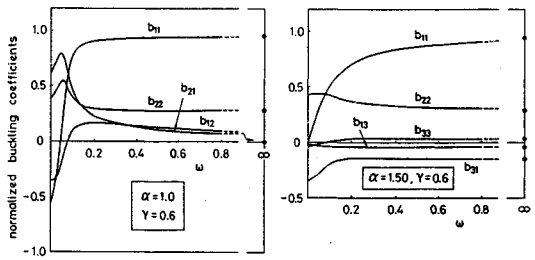

Fig.4 Change of buckling mode with ω.

into account by the first term of Eq. (14). This result strongly suggests that the critical shear stress in design should be evaluated by τ_{av} rather than τ_a for the interactive buckling strength, and supports the validity of shear force calculated in Ref. 20).

(4) Buckling coefficient

Fig.3 shows the relation between the aspect ratio α and the buckling coefficient $k_{\sigma 2}$ defined by

$$k_{\sigma 2} \equiv \frac{6\,(M_2)_{cr}}{\pi^2 D} \quad \cdots\cdots (16)$$

As ω becomes small, the buckling coefficient is likely to be influenced by the higher-order buckling modes of bending type. This effect can be clearly recognized especially when $\omega=0.0$ and $\gamma=1.0$. As ω becomes larger, the smooth and monotonically decreasing curves are obtained. This indicates that the shear buckling mode becomes dominant in the interactive buckling phenomena. The conventional loading of pure bending and pure shear yields the most conservative buckling strength. This fact stands by the validity of conventional calculation of the interactive buckling strength in the engineering sense.

From a practical point of view, it is quite useful to express the buckling coefficient $k_{\sigma 2}$ explicitly in terms of α, γ and ω. By the analogy with the conventional formulas to predict the pure shear and pure bending buckling strength, we choose the following expression :

$$k_{\sigma 2} = \frac{a_1}{\alpha^2} + a_2 \quad \cdots\cdots (17)$$

At first, the original curves in **Fig.3** are redrawn approximately by the smooth envelopes. These envelopes are then regressed in the form of Eq. (17) to obtain the coefficients a_1 and a_2 as tabulated in **Table 1**. Next, these coefficients are again regressed in terms of γ and ω. If a cubic polynomial is chosen for γ and ω, the obtained expressions for a_1 and a_2 are given by

for $0.0 \leqq \omega \leqq 0.5$:

$$\begin{cases} a_1 = 2.240 - 1.567\gamma + 5.929\omega - 2.448\gamma^2 \\ \quad + 8.890\omega^2 + 3.079\gamma\omega + 1.962\gamma^3 - 4.105\gamma^2\omega \\ \quad + 8.136\gamma\omega^2 - 30.051\omega^3 \quad [0.995], \\ a_2 = 29.750 - 0.479\gamma - 53.595\omega - 4.010\gamma^2 \\ \quad - 25.653\omega^2 + 28.587\gamma\omega - 1.464\gamma^3 \\ \quad + 12.220\gamma^2\omega - 54.791\gamma\omega^2 + 107.976\omega^3 \\ \quad [0.999] \end{cases} \quad \cdots\cdots (18\text{-a,b})$$

for $0.5 < \omega \leqq 4.0$:

$$\begin{cases} a_1 = 4.817 - 2.011\omega - 0.967\gamma^2 + 0.274\omega^2 \\ \quad + 0.724\gamma\omega + 0.282\gamma^2\omega - 0.188\gamma\omega^2 \ [0.997], \\ a_2 = 18.205 + 1.474\omega - 21.442\omega + 0.233\gamma^2 \\ \quad + 9.336\omega^2 - 1.186\gamma\omega - 0.152\gamma^3 + 0.201\gamma\omega^2 \\ \quad - 1.259\omega^3 \quad [0.999] \end{cases} \quad \cdots\cdots (18\text{-c,d})$$

in which $a_1 \geqq 0$ and $a_2 \geqq 0$ must be kept in both cases. The numerals in [ ] give the correlation coefficients. The effective range of γ, ω and α in the above equations are $0 \leqq \gamma \leqq 1.0$, $0 \leqq \omega \leqq 4.0$ and $0.5 \leqq \alpha \leqq 3.0$, respectively. The estimated buckling coefficients $k_{\sigma 2}$ by Eqs. (17) and (18) are also

Table 1 Regression coefficients a_1 and a_2.

	ω	0.0	0.05	0.1	0.2	0.3	0.4	0.5	0.6	0.8	1.0	2.0	4.0
γ=0.0	a_1	2.249	2.463	2.935	3.583	3.903	3.999	3.854	3.714	3.376	3.049	1.969	1.124
	a_2	29.746	27.303	23.973	18.509	14.506	11.577	9.726	8.261	6.307	5.076	2.529	1.248
γ=0.2	a_1	1.937	2.029	2.654	3.591	3.857	3.981	3.906	3.785	3.456	3.125	2.010	1.140
	a_2	29.389	27.608	24.422	18.622	14.946	11.983	9.965	8.440	6.413	5.144	2.542	1.250
γ=0.4	a_1	1.467	1.517	1.985	3.098	3.598	3.835	3.853	3.774	3.487	3.170	2.046	1.154
	a_2	28.328	27.250	24.624	19.281	15.419	12.357	10.215	8.633	6.533	5.221	2.557	1.252
γ=0.6	a_1	0.958	0.974	1.445	2.583	3.275	3.570	3.695	3.679	3.464	3.180	2.075	1.168
	a_2	27.126	26.551	24.490	19.524	15.509	12.690	10.462	8.836	6.664	5.309	2.575	1.255
γ=0.8	a_1	0.528	0.590	1.044	1.975	2.865	3.255	3.450	3.507	3.388	3.153	2.097	1.181
	a_2	25.615	25.150	23.432	19.305	15.593	12.860	10.686	9.034	6.805	5.405	2.596	1.258
γ=1.0	a_1	0.315	0.435	0.776	1.588	2.381	2.898	3.136	3.277	3.262	3.090	2.111	1.192
	a_2	23.623	23.201	21.966	18.739	15.495	12.803	10.833	9.213	6.947	5.510	2.619	1.261

Remarks : $k_{\sigma 2} = \frac{a_1}{\alpha^2} + a_2$, $\sigma_{2cr} = k_{\sigma 2} \frac{\pi^2 E}{12(1-\nu^2)}(\frac{1}{\beta})^2$.

[$k_{\sigma 2}$]: buckling coefficients, [α]: aspect ratio of a panel;a/b, [β]: depth-thickness ratio;b/t, [γ]: ratio of unequal end moments;M_1/M_2, [ω]: ratio of applied bending stress and shear stress;τ_a/σ_{x2}.

shown in **Fig.3** by the dashed curves. These curves can estimate the actual buckling coefficients fairly well, but unconservative estimation occurs in some cases. However, these errors can be diminished by the choice of the higher-order polynomials.

Furthermore, **Fig.4** shows the relationships between the normalized buckling mode b_{mn} and ω. The case of $\omega=\infty$ corresponds to the pure shear condition, and the case of $\omega=0$ to the bending with no external shear forces. Each mode approaches rapidly to that of pure shear buckling mode as ω becomes large. Therefore, the interactive buckling phenomena is governed mostly by the shear even when the bending moments are acting.

3. POST-BUCKLING BEHAVIOR OF A PANEL UNDER COMBINED LOADING

(1) Analytical solution of Marguerre's equation

Marguerre's equations[21] for the plate bending with relatively large deflection are expressed in terms of the out-of-plane deflection $w(x, y)$, initial deflection $w_0(x, y)$ and stress function $F(x, y)$ as

$$\nabla^4 w=\frac{t}{D}\left[\frac{\partial^2 F}{\partial y^2}\frac{\partial^2(w+w_0)}{\partial x^2}+\frac{\partial^2 F}{\partial x^2}\frac{\partial^2(w+w_0)}{\partial y^2}-2\frac{\partial^2 F}{\partial x\partial y}\frac{\partial^2(w+w_0)}{\partial x\partial y}\right] \quad \cdots\cdots (19\text{-a})$$

$$\nabla^4 F=E\left\{\left[\frac{\partial^2(w+w_0)}{\partial x\partial y}\right]^2-\frac{\partial^2(w+w_0)}{\partial x^2}\frac{\partial^2(w+w_0)}{\partial y^2}-\left(\frac{\partial^2 w_0}{\partial x\partial y}\right)^2+\frac{\partial^2 w_0}{\partial x^2}\frac{\partial^2 w_0}{\partial y^2}\right\} \quad \cdots\cdots (19\text{-b})$$

Since the four edges are simply supported, the deflections can be expressed in the same manner as Eq. (3) by

$$w_0=t\sum_{m=1}^{\infty}\sum_{n=1}^{\infty}a_{mn}\sin\left(\frac{m\pi x}{a}\right)\sin\left(\frac{n\pi y}{b}\right),$$

$$w=t\sum_{m=1}^{\infty}\sum_{n=1}^{\infty}b_{mn}\sin\left(\frac{m\pi x}{a}\right)\sin\left(\frac{n\pi y}{b}\right) \quad \cdots\cdots (20\text{-a,b})$$

where a_{mn}'s are given quantities of the initial deflection, and b_{mn}'s are the unknown coefficients to be determined. In this case, the expression of F can be obtained by addition of the homogeneous solution Eq. (5) and a particular solution corresponding to the right-hand-side of Eq. (19-b) using Eq. (20) as

$$F=\tau_a\cdot xy-\frac{(2y^3-3by^2)}{b^3 t}\left\{M_1+(M_2-M_1)\frac{x}{a}\right\}+Et^2\sum_{p=0}^{\infty}\sum_{q=0}^{\infty}\phi_{pq}\cos\left(\frac{p\pi x}{a}\right)\cos\left(\frac{2q\pi y}{b}\right) \quad \cdots\cdots (21)$$

It should be noted that a mechanical boundary condition of Eq. (4-d) is here relaxed to $\int_0^a \sigma_y dx=0$. Then, Eq. (21) satisfies all the boundary conditions of Eq. (4) in this sense. The elongation in the x-direction results in a linear function of y as

$$[u]_{x=a}-[u]_{x=0}=\int_0^a \frac{\partial u}{\partial x}dx$$

$$=\int_0^a\left\{\frac{1}{E}(\sigma_x-\nu\sigma_y)-\frac{1}{2}\left(\frac{\partial w}{\partial x}\right)^2-\left(\frac{\partial w}{\partial x}\right)\left(\frac{\partial w_0}{\partial x}\right)\right\}dx$$

$$=-\frac{3a(2y-b)}{Eb^3t}(M_1+M_2)$$

$$-\frac{t^2\pi^2}{8a}\sum_{m=1}^{\infty}\sum_{n=1}^{\infty}m^2b_{mn}(b_{mn}+2a_{mn})$$

Substituting Eqs. (20) and (21) into Eq. (19-b), we obtain the expression of ϕ_{pq}[22] in terms of a_{mn} and b_{mn} as

$$\frac{8(p^2+4\alpha^2q^2)^2}{\alpha^2}\phi_{pq}=\sum_{m=1}^{\infty}\sum_{n=1}^{\infty}\sum_{i=1}^{\infty}\sum_{j=1}^{\infty}(a_{mn}b_{ij}+b_{mn}a_{ij}$$

$$+b_{mn}b_{ij})\{2mnij\pm(m^2j^2+n^2i^2)\} \quad \cdots\cdots (22)$$

$$-: \begin{cases} p=m+i \text{ and } q=(n+j)/2 \\ \text{or} \\ p=|m-i| \text{ and } q=|n-j|/2 \end{cases},$$

$$+: \begin{cases} p=|m-i| \text{ and } q=(n+j)/2 \\ \text{or} \\ p=m+i \text{ and } q=|n-j|/2 \end{cases},$$

where p and q are positive integers. Final equation to be solved with Eq. (22) can be obtained by direct substitution of Eqs. (20) and (21) into Eq. (19-a), but becomes too complicated. Therefore, Galerkin's method[10)-13),21),23),24)] is applied to Eq. (19-a) as

$$\int_0^a\int_0^b\left\{\nabla^4 w-\frac{t}{D}\left[\frac{\partial^2F}{\partial y^2}\frac{\partial^2(w+w_0)}{\partial x^2}\right.\right.$$

$$\left.\left.+\frac{\partial^2F}{\partial x^2}\frac{\partial^2(w+w_0)}{\partial y^2}-2\frac{\partial^2F}{\partial x\partial y}\frac{\partial^2(w+w_0)}{\partial x\partial y}\right]\right\}$$

$$\sin\left(\frac{r\pi x}{a}\right)\sin\left(\frac{s\pi y}{b}\right)dxdy=0, \quad r,s=1,2,3,.... \quad \cdots\cdots (23)$$

By substituting Eqs. (20) and (21) into Eq. (23) and integrating it, we obtain the following fundamental equations :

$$\frac{\pi^4}{4\alpha^2}(r^2+\alpha^2s^2)^2b_{rs}$$

$$-6(\lambda_2+\lambda_1)\sum_{n+s}(a_{rn}+b_{rn})\frac{r^2ns}{(n^2-s^2)^2}[(-1)^{n+s}-1]$$

$$+\frac{24}{\pi^2}(\lambda_2-\lambda_1)\sum_{m+r}\sum_{n+s}(a_{mn}+b_{mn})\cdot$$

$$\frac{mnrs(r^2s^2-m^2n^2+3n^2r^2-3m^2s^2)}{(r^2-m^2)^2(s^2-n^2)^3}\cdot$$

$$[(-1)^{m+r}-1][(-1)^{n+s}-1]$$

$$+2\alpha\lambda_3\sum_{m+r}\sum_{n+s}(a_{mn}+b_{mn})\frac{mnrs}{(r^2-m^2)(s^2-n^2)}\cdot$$

$$[(-1)^{m+r}-1][(-1)^{n+s}-1]$$

$$-\frac{3}{4}(1-\nu^2)\pi^4\sum_{m=1}^{\infty}\sum_{n=1}^{\infty}(a_{mn}+b_{mn})\cdot$$

$$\{[m(n+s)-n(m+r)]^2\phi_{m+r,\frac{n+s}{2}}$$
$$-[m(n+s)-n(m-r)]^2\phi_{m-r,\frac{n+s}{2}}$$
$$-[m(n+s)+n(r-m)]^2\phi_{r-m,\frac{n+s}{2}}$$
$$-[m(n-s)-n(m+r)]^2\phi_{m+r,\frac{n-s}{2}}$$
$$+[m(n-s)-n(m-r)]^2\phi_{m-r,\frac{n-s}{2}}$$
$$+[m(n-s)+n(r-m)]^2\phi_{r-m,\frac{n-s}{2}}$$
$$-[m(s-n)+n(m+r)]^2\phi_{m+r,\frac{s-n}{2}}$$
$$+[m(s-n)+n(m-r)]^2\phi_{m-r,\frac{s-n}{2}}$$
$$+[m(s-n)-n(r-m)]^2\phi_{r-m,\frac{s-n}{2}}\}$$
$$=0, \quad r,s=1,2,3,..... \quad \cdots\cdots (24)$$

where ϕ_{pq}'s are zero when $p<0$ or $q<0$, and the following non-dimensional expressions are introduced :

$$\lambda_1\equiv\frac{M_1}{D}, \quad \lambda_2\equiv\frac{M_2}{D}, \quad \lambda_3\equiv\frac{\tau_a b^2t}{D} \quad \cdots\cdots (25\text{-a})$$

Then the parameters in Eq. (6) can be rewritten as

$$\gamma=\frac{\lambda_1}{\lambda_2}, \quad \omega=\frac{\lambda_3}{6\lambda_2}. \quad \cdots\cdots (25\text{-b})$$

Eq. (24) results in a set of third-order simultaneous algebraic equations of b_{mn}, and the Newton-Raphson method is employed to solve. Substitution of obtained b_{mn} into Eq. (20-b) yields the out-of-plane deflection in the post-buckling state.

(2) Post-buckling behavior

In the series above, the first five terms are used in this iterative calculation. This choice yields less than 1 % difference in deflection and 9 % error locally in maximum stress from those results obtained by using seven terms. Load increment is set $1.0\times M_2/D$ in order to avoid the numerical instability and adjusted to be $0.5\times M_2/D$ if necessary.

Fig.5 shows typical load-deflection curves after buckling when $w_0=0$. The deflection is calculated at a point, $x=0.35a$ and $y=0.70b$, indicated by a dot in the inset of the figure. After buckling, the out-of-plane deformation begins to develop, but the deflection paths are smooth. **Fig.6** also shows similar curves for a different set of parameters, but a jump is observed when $\omega=0.1333$. There exists an instability point[25)] on this path beyond the buckling load, and further investigations are required for complete understanding.

Typical deformed configurations are shown in **Fig.7** with those in the case of the pure bending and pure shear loading. In the case of combined loading, deformed configuration is composed of the mixed mode of bending and shear, and is greatly affected by the parameters α, γ and ω.

Fig.8 depicts the distributions of the stress components σ_x, σ_y and τ_{xy} along the several sections inside the panel. These stresses are normalized by the tensile yield stress $\sigma_Y=235$

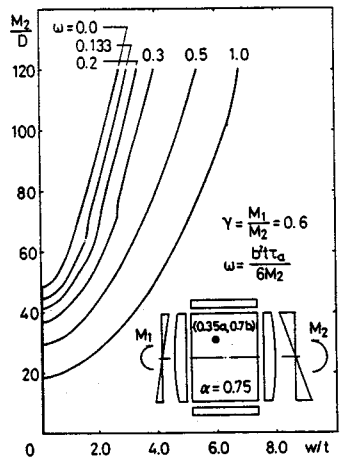

Fig.5 Typical load-deflection curves after buckling for given ω.

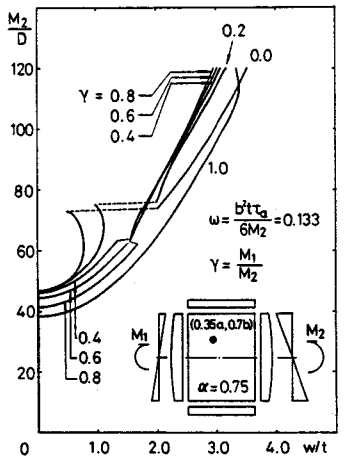

Fig.6 Typical load-deflection curves after buckling for given γ.

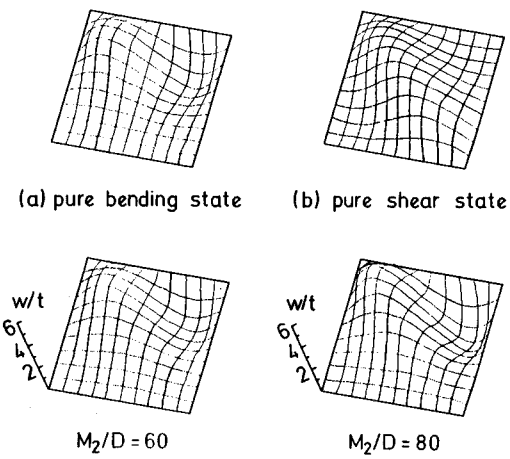

Fig.7 Deformed configurations of a panel after buckling.

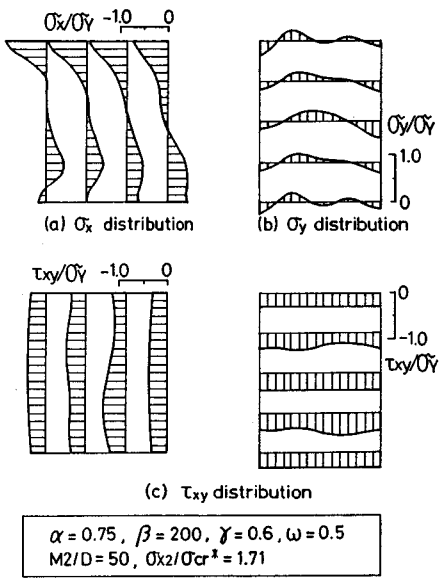

Fig.8 Stress distributions of a panel after buckling.

MN/m² to evaluate what extent the nonlinearity of stress distribution appear before the yielding of material. The bending stress σ_x no longer distributes linearly after buckling, and the stress redistribution occurs in the upper half depth of the section where the compressive stresses are acting in advance of the yielding. Since this analysis is limited for a web panel, the effect of flanges may cause somewhat different stress distribution in the actual plate girders.

The transverse stress component σ_y becomes larger after buckling, and becomes in the same order of magnitude of the other stress components. The shear stress τ_{xy} always satisfies the mechanical boundary condition, but varies inside the panel as shown in **Fig.**8 (c).

Fig.9 shows the development of the principal stresses at the center of a panel ($x=0.5a$, $y=0.5b$). While the tensile principal stresses increase monotonically, the compressive principal stresses increase up to the buckling load and then decreases its slope. In both cases of $\alpha=0.75$ and $\omega=0.133$ or $\alpha=1.25$ and $\omega=0.5$, somewhat different behavior is observed ; i.e. the curve is non-smooth when the larger bending moment is applied. There again might exist an instability point like in **Fig.**8.

The principal stress distribution for the case of $\alpha=1.25$, $\gamma=0.6$, $\omega=0.5$ and $M_2/D=50$ is repre-

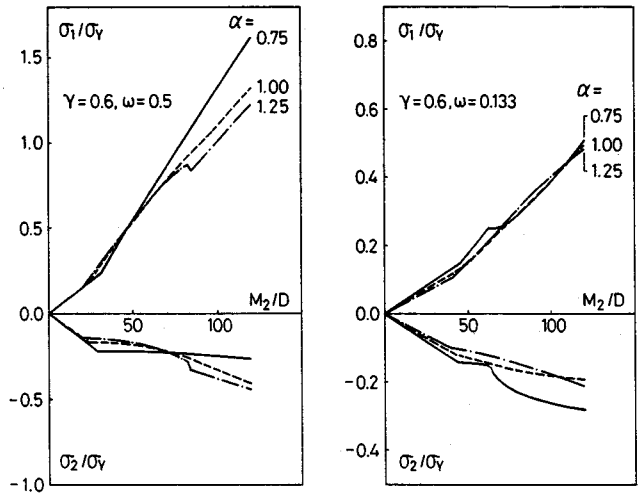

Fig.9 Development of principal stresses.

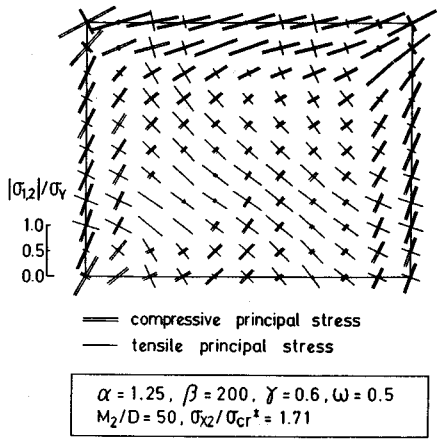

Fig.10 Principal stress distribution.

sented in **Fig.10**. Since the compressive principal stresses are concentrated near the joint region between the compressive flange and the web plate due to the stress redistribution after buckling, the yielding will generally be initiated at this portion. Furthermore, the so-called gusset plate action is observed in the upper corner region of the left-hand-side on which the smaller end moment M_1 is applied. Namely, larger compressive principal stresses co-exist with the tensile ones in this corner.

4. CONCLUSION

In order to examine the realistic behavior of a panel subjected to the combined unequal bending and shear in the actual plate girder structures, an Airy's stress function is derived, and the buckling strength and post-buckling behavior is investigated semi-analytically.

(1) When the applied shear stress is correctly evaluated by τ_{av} including the effect of unequal moments, the conventional interaction formula almost gives the conservative buckling strength. Therefore, it is suggested that the applied shear stress should be always defined by τ_{av} for the interactive buckling strength. Moreover, a simple-form formula to predict more exact buckling coefficients under combined unequal bending and shear is presented.

(2) In the most interactive buckling phenomena, the shear mode is dominant. Each mode approaches rapidly to the pure shear buckling mode as ω becomes large. The out-of-plane deflection after such a buckling is composed of the mixed mode of bending and shear.

(3) After buckling, the bending stress distributions σ_x show the lack of compressive stresses in the upper part of the panel depth due to the redistribution effect. The shear stress τ_{xy} always satisfies the mechanical boundary conditions at the boundary and shows a little disturbed distributions inside the panel. On the other hand, the transverse stress σ_y emerges after buckling and can not be neglected any more.

(4) The principal stress distribution shows the stress concentration near the joint region between the compressive flange and the web plate, which will cause the initiation of yielding. The gusset plate action is also recognized in the corner region.

5. ACKNOWLEDGMENT

The authors would like to thank Mr. Takeshi SASAKI, Iwate Prefectural Office, for assistance of the numerical calculations. This study was supported in part by the Grant-in-Aid for Encouragement of Young Engineers and Scientists from the Society for the Promotion of Construction Engineering (Chairman of the board of directors, Professor Nobuo SHUTO, Tohoku University) in 1989.

REFERENCES

1) Stein, O.: Die Stabilität der Blechträgerstehbleche im zweiachsigen Spannungszustand, Der Stahlbau, Heft 8, S.57～60, 1934.
2) Chwalla, E.: Beitrag zur Stabilitätstheorie des Stegbleches vollwandiger Träger, Der Stahlbau, Heft 21/22, S.161～166, 1936.
3) Timoshenko, S.P.: The stability of the webs of plate girders, Engineering, Vol.138, pp.207～209, 1934.
4) Way, S.: Stability of rectangular plates under shear and bending forces, Journal of Applied Mechanics, Vol.3, No.4, pp.A 131～A 135, 1936.
5) Nölke, K.: Biegungs-beulung der Rechteckplatte mit Eingespannten Längsrändern, Der Bauingenieur, Heft

13/14, S.111, 1936.

6) Young, D.: Analysis of clamped rectangular plates, Journal of Applied Mechanics, Vol.7, No.4, pp.A 139～A 142, 1940.
7) Levy, S.: Buckling of rectangular plates with built-in edges, Journal of Applied Mechanics, Vol.9, No.4, pp.A 171～A 174, 1942.
8) Woolley, R.M., Corrick, J.N. and Levy, S.: Clamped long rectangular plate under combined axial load and normal pressure, NACA Technical Report No.1047, 1946.
9) Moriwaki, Y. and Nara, S.: Buckling strength of web plates of plate girders under in-plane combined loading, Journal of Structural Engineering, JSCE, Vol.35 A, pp.127～134, 1989 (in Japanese).
10) Radulović, B.: Beitrag zur Stabilität einer Rechteckplatte, die einer in beiden Richtungen über die Plattenebene linear veränderlichen Last unterworfen ist, bei Navierschen Randbedigungen, Der Stahlbau, 42. Jahrgang, (Heft 7, S.199～205), (Heft 12, S.384), 1973.
11) Radulović, B.: Über die Quersteifungen einer Rechteckplatte, die einer in beiden Richtungen über die Plattenebene linear veränderlichen Last unterworfen ist, Der Stahlbau, 43. Jahrgang, Heft 4, S.120～124, 1974.
12) Radulović, B.: Über die Längsversteifungen einer Rechteckplatte, die einer in beiden Richtungen über die Plattenebene linear veränderlichen Last unterworfen ist, Der Stahlbau, 45. Jahrgang, Heft 8, S.230～237, 1976.
13) Radulović, B.: Einfluß der Torsionssteifigkeit der Aussteifungen zur Stabilität einer Rechteckplatte, die einer in beiden Richtungen über die Plattenebene linear veränderlichen Last unterworfen ist (lineare Beultheorie), Der Stahlbau, 47. Jahrgang, Heft 7, S.212～216, 1978.
14) Kutzelnigg, E.: Beulwertdiagramme für Stegbleche ohne Zwischensteifen nach der linearen Beultheorie bei Berücksichtigung von in Trägerlängsrichtung veränderlichen Spannungen und der Torsionssteifigkeit der Trägergurte, Der Stahlbau, 47. Jahrgang, Heft 11, S.329～338, 1978.
15) Takeda, H., Mikami, I. and Yonezawa, H.: Elastic lateral buckling of plate girder, Theoretical and Applied Mechanics, University of Tokyo Press, Vol.24, pp.343～355, 1974.
16) Timoshenko, S.P. and Gere, J.M.: Theory of Elastic Stability, 2 nd Ed., pp.319～385, McGraw-Hill, New York, 1961.
17) Japan Society of Civil Engineers: Guidelines for Stability Design of Steel Structures, Subcommittee on Stability Design Committee on Steel Structures (ed. by Fukumoto, Y.), 1987 (in Japanese).
18) Japan Society of Civil Engineers, Kansai Branch: Research and Study Report on the Strength and Design of Steel Plated Structures (ed. by Mikami, I.), 1988, 1989 (in Japanese).
19) Column Research Council of Engineering Foundation: Guide to Stability Design Criteria for Metal Structures, 4 th Ed. (ed. by T.V. Galambos), p.112, New York, John Wiley & Sons Inc., 1988.
20) Japan Road Association: Specifications for Highway Bridges, Steel Bridges, 1990 (in Japanese).
21) Yamaki, N.: Postbuckling behavior of rectangular plates with small initial curvature loaded in edge compression, Journal of Applied Mechanics, Trans. ASME, Vol.26, pp.407～414, 1959.
22) Usami, T.: Post-buckling of plates in compression and bending, J. Struct. Div., Proc. ASCE, Vol.108, No.ST 3, pp.591～609, 1982.
23) Coan, J.M.: Large deflection theory for plates with small initial curvature loaded in edge compression, Journal of Applied Mechanics, Vol.18, pp.143～151, 1951.
24) Konishi, I., Shiraishi, N. and Watanabe, E.: A consideration on the strength of webplates, Proc. JSCE, No.136, pp.15～23, 1966 (in Japanese).
25) Fujii, K. *et al.*: Elastic large deformation behavior of a web panel in the curved girder under bending, Proceedings of the 42nd Annual Conference, JSCE, Vol. I , pp.130～131, 1987 (in Japanese).

(Received July 16, 1990)

不等曲げとせん断を受けるパネルの弾性座屈強度および後座屈挙動

中沢正利・岩熊哲夫・倉西　茂

本研究では，不等曲げとせん断の組合せ荷重を受ける単純支持板の弾性連成座屈強度および後座屈挙動を解析的に調べている．現実の桁構造で起こり得る状態を想定し，パネル両端での不等曲げモーメントの効果に特に着目している．連成座屈現象は主にせん断座屈モードの影響を強く受けることが明らかにされた．さらに，連成荷重下での弾性後座屈挙動および応力分布についても論じている．